Evaluation of Bioprinted Autologous Cartilage Grafts in an Immunocompetent Rabbit Model

Author(s):
Gvaramia, David; Fisch, Philipp; Flégeau, Killian; Huber, Lena; Kern, Johann; Jakob, Yvonne; Hirsch, Daniela; Rotter, Nicole

Publication date:
2024

Permanent link:
https://doi.org/10.3929/ethz-b-000667013

Originally published in:
Advanced Therapeutics, https://doi.org/10.1002/adtp.202300441

Funding acknowledgement:
173868 - Sinergia Project: A Tissue, Cell and Molecular Approach to Understanding and Treating Microtia (SNF)

ADVANCED THERAPEUTICS
www.advtherap.com

Evaluation of Bioprinted Autologous Cartilage Grafts in an Immunocompetent Rabbit Model

*David Gvaramia, Philipp Fisch, Killian Flégeau, Lena Huber, Johann Kern, Yvonne Jakob, Daniela Hirsch, and Nicole Rotter**

The gold standard of auricular reconstruction involves manual graft assembly from autologous costal cartilage. The intervention may require multiple surgical procedures and lead to donor-site morbidity, while the outcome is highly dependent on individual surgical skills. A tissue engineering approach provides the means to produce cartilage grafts of a defined shape from autologous chondrocytes. The use of autologous cells minimizes the risk of host immune response; however, factors such as biomaterial compatibility and in vitro maturation of the tissue-engineered (TE) cartilage may influence the engraftment and shape-stability of TE implants. Here, this work tests the biocompatibility of bioprinted autologous cartilage constructs in a rabbit model. The TE cartilage is produced by embedding autologous auricular chondrocytes into hyaluronan transglutaminase (HATG) based bioink, previously shown to support chondrogenesis in human auricular chondrocytes in vitro and in immunocompromised xenotransplantation models in vivo. A drastic softening and loss of cartilage markers, such as sulfated glycosaminoglycans (GAGs) and collagen type II are observed. Furthermore, fibrous encapsulation and partial degradation of the transplanted constructs are indicative of a strong host immune response to the autologous TE cartilage. The current study thus illustrates the crucial importance of immunocompetent autologous animal models for the evaluation of TE cartilage function and compatibility.

1. Introduction

The need for auricular cartilage reconstruction can occur due to hereditary conditions, such as microtia or anotia, trauma, malignancies, and infections.[1–3] The current gold standard for restoring or reconstructing the pinna is the use of autologous rib cartilage, which is hand-carved by the surgeon to obtain the shape of the auricle.[3] The procedure is highly skill-dependent and tedious, often requiring multiple stages of surgery.[2] The use of high-density polyethylene implants such as Medpor is the most common clinically used alternative to autologous cartilage.[4] In both cases, the aesthetic result does not always match the natural shape and/or mechanical properties of the auricle. Complications such as donor site morbidity or implant extrusion are common.[2]

Tissue engineering provides an alternative approach, where the patient's own cells obtained from a small biopsy can be used to produce auricular cartilage, bioprinted or molded into the desired shape to

D. Gvaramia, J. Kern, Y. Jakob, N. Rotter
Department of Otorhinolaryngology
Head and Neck Surgery
Medical Faculty Mannheim
University of Heidelberg, Germany
E-mail: Nicole.rotter@medma.uni-heidelberg.de

P. Fisch, K. Flégeau
Tissue Engineering and Biofabrication Laboratory
Institute for Biomechanics
ETH Zurich, Switzerland

L. Huber, N. Rotter
Department of Otorhinolaryngology
Head and Neck Surgery
University Medical Center Mannheim
University of Heidelberg, Germany

D. Hirsch
Institute of Pathology
University of Regensburg
Regensburg, Germany

The ORCID identification number(s) for the author(s) of this article can be found under https://doi.org/10.1002/adtp.202300441

DOI: 10.1002/adtp.202300441

symmetrically match the healthy ear (e.g., in case of unilateral reconstruction).[5,6] Typically, chondrocytes are embedded in hydrogels to provide a hydrated 3D environment that resembles the composition of the cartilage extracellular matrix (ECM) and maintains the round morphology of the encapsulated cells.[7] When successful, this results in de novo production of cartilage ECM and the formation of tissue with biomechanical and biochemical properties similar to native cartilage. However, achieving cartilage-like ECM is highly complicated, particularly due to the dedifferentiation of chondrocytes and the concomitant formation of fibrocartilage. Therefore, recent studies combine the tissue engineering approach with the 3D printing of external scaffolds to provide additional stability and the potential to produce personalized shapes for engineered cartilage.[8]

Long-term shape stability of such tissue-engineered (TE) constructs is typically tested in vivo, in immunocompromised xenograft animal models, such as nude mice, to prevent the immune response to human TE grafts.[9] However, autologous transplantation of TE constructs into an immunocompetent animal model remains the ultimate preclinical test to assess their safety and efficiency, and is a prerequisite for further clinical testing and implementation of TE products.[4,10] The immune response is typically caused by the biomaterial or products of its degradation.[11] Beyond the conventional biomaterial compatibility experiments, autologous animal models also provide insight into the influence of cells and cell-produced bioactive components (ECM, cytokines) on the host response to the TE graft. Pre-culturing of TE constructs before their transplantation has been described to mitigate the host immune response through partial degradation of the biomaterial and its substitution with the cell-produced ECM during the in vitro culture. In addition, cell-produced components might partially cover the scaffold thus masking the biomaterial and reducing host tissue response to it.[10,12]

Establishing an autologous model for TE products remains a major challenge. The outcomes of such experiments can depend on the choice of animals, biomaterials, and site of the transplantation, among other factors.[11] While rodents are the most practical choice for the majority of in vivo experiments, they rarely satisfy criteria for an autologous model, such as sufficient cell yield required for a TE construct or the size of the animal, which can accommodate a human-scale organ, such as the auricle. For testing the biocompatibility and shape stability of large TE constructs, the use of larger animals, such as rabbit,[9,13,14] swine,[15,16] and sheep[10,17,18] have been proposed.

Most studies with autologous transplantation of TE cartilage into immunocompetent animal models have employed conventional, commercially available synthetic or biological materials such as polyglycolic acid (PGA) and polycaprolactone (PCL),[6,9,12,15] pluronic,[15,19] chitosan,[16] alginate,[15,18] and collagen[10,17] with mixed success regarding the quality of the TE construct or the outcome of the transplantation. Resorption of the TE cartilage, poor shape stability, calcification, excessive immune response, and degradation associated with the material have all been commonly reported.[2,4,5] The use of natural biodegradable materials is advisable to mitigate the host immune response.[20] Furthermore, with the advancement of bioprinting, rheological properties and printability of biomaterials are increasingly gaining relevance. Bioprinting facilitates replication of complex anatomical structures such as human auricle with high precision but requires adequate viscosity of the bioink, without damaging the embedded cells and providing favorable environment for tissue maturation.

Here, we used a hyaluronan transglutaminase (HATG) based bioink to bioprint constructs containing autologous rabbit auricular chondrocytes. HATG, hyaluronan modified with transglutaminase substrate peptides for cross-linking with factor XIII, was previously shown to support cartilage maturation in vitro and in vivo.[21,22] In addition, HATG can be bioprinted using calcium-triggered enzymatic cross-linking which is suitable in combination with alginate.[23] Previous studies have shown good print fidelity, high cell viability post printing, and the creation of complex three-dimensional shapes such as the auricle.[23,24]

Recent studies have highlighted the benefit of alginate on the chondrogenic capacity of chondrocytes.[25] We, therefore, developed a bioink based on HATG and alginate and bioprinted cylindrical grafts for subcutaneous implantation in an autologous rabbit model. To decouple the influence of the implant shape, which can potentially lead to complications such as seroma,[26,27] from the immune response to the material, cylindrical grafts were printed. Bioprinting, however, allows the creation of complex, anatomical grafts such as the auricle by adapting the printing process based on patient-specific 3D models. Such complex models were bioprinted and implanted in immunocompromised animals in previous studies,[23,24] but due to the lack of an intact immune system, no conclusion on the complex immune response could be drawn. Understanding the host immune response toward TE constructs is crucial for successful clinical translation of the tissue engineering field.

2. Experimental Section

2.1. Surgical Procedures and the Animal Model

Four female New Zealand 14- to 16-week-old white rabbits were purchased from Charles River Laboratories (Sulzfeld, Germany). The ethical approval for the animal study was issued by the regional authority in Karlsruhe (35-9185.81/G-43/21). Six additional rabbit auricular cartilage biopsies were acquired from an unrelated study and used for bioprinting constructs for the in vitro evaluation only. Thus, the total number of animals for the in vitro maturation analysis constituted a total of 10 donors (**Figure 1b**).

All surgeries were performed in sterile conditions, under general anesthesia induced by subcutaneous (s.c.) injection of Medetomidine 0.2 mg kg^{-1}, Midazolam 1 mg kg^{-1}, and Fentanyl 0.02 mg kg^{-1} (MMF mixture) and maintained by incremental injection of 0.1–0.2 mL MMF (diluted 1:3 in NaCl 0.9%) through the ear vein while monitoring breathing frequency and reflexes.

Auricular cartilage of approximately 2 × 2 cm was harvested through an incision on the anterior surface of the auricle (Figure 1a, **Figure 2a–c**) following the subcutaneous infiltration of the biopsy site with lidocaine 1% with Epinephrine 1:100 000. The surrounding connective tissue and perichondrium were removed from the cartilage by blunt dissection and the biopsies were transferred to sterile NaCl 0.9% for further processing and cell isolation. The skin was closed with sutures and subsequent tissue adhesive application (Surgibond, SMI).

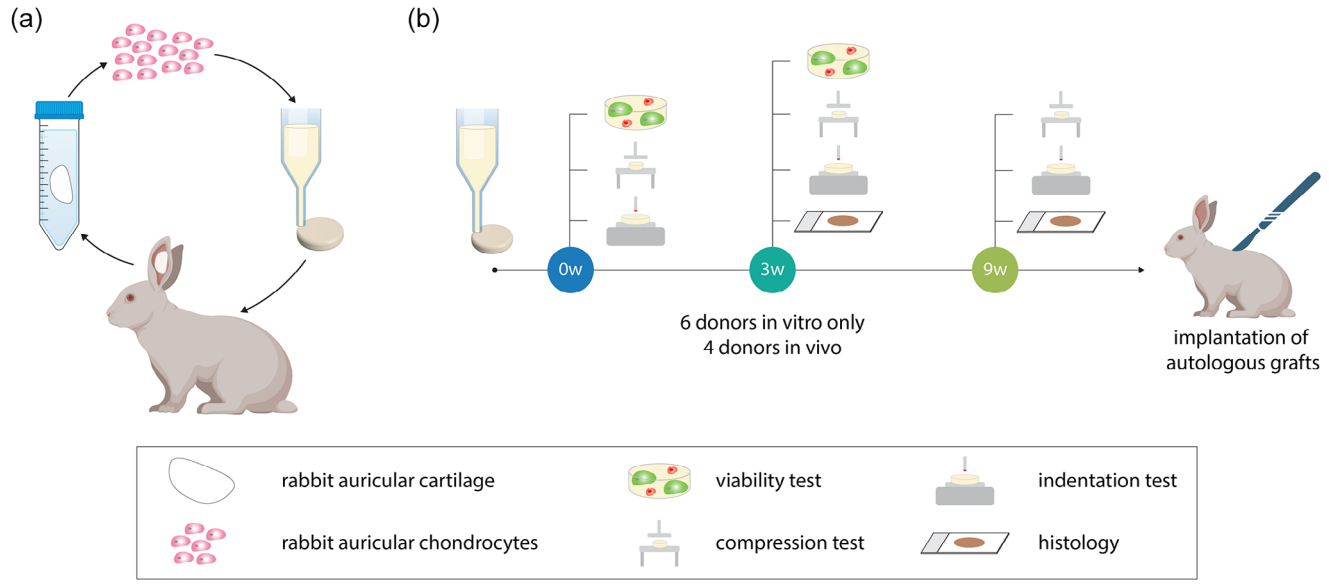

Figure 1. Schematic depiction of the study layout. a) Schematic illustration of autologous cartilage preparation and transplantation from an auricular cartilage biopsy. b) The sequence of experiments performed for the analysis of the autologous bioprinted cartilage grafts during the in vitro maturation period. Afterwards, the grafts were implanted for 14 weeks in rabbits. Figure created with the support of BioRender.com.

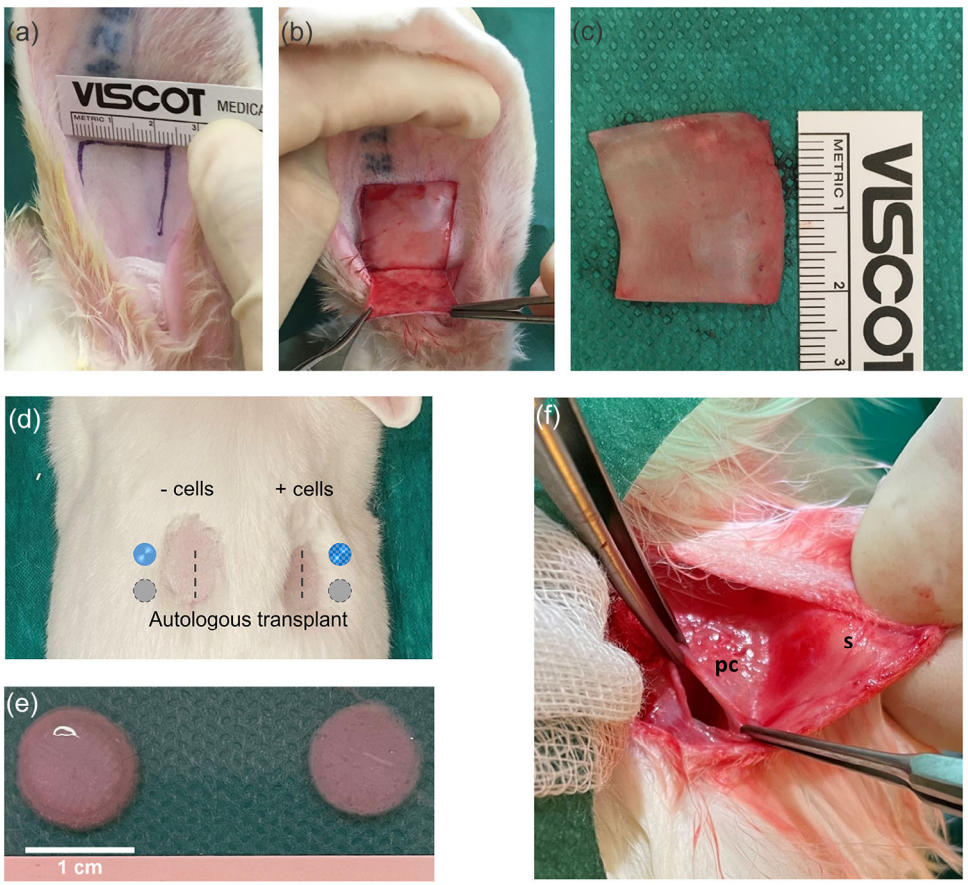

Figure 2. Surgical Procedures. a) The site of the biopsy (marked) at the anterior surface of the auricle before and b) after skin dissection. c) The excised cartilage biopsy used to obtain autologous chondrocytes. d) The areas of incision (dashed lines) at the back of the rabbits prepared for the implantation of two constructs and one autologous control on each side. e) A photograph depicting the cylinders before the implantation. f) Implantation pocket created subcutaneously in the panniculus carnosus (PC). s – skin.

At the second stage of the experiment, the TE cylinders with or without autologous cells (two cylinders per condition) were prepared as described below and implanted on the back of the rabbits for 14 weeks (Figure 2d–f). Panniculus carnosus (PC) was accessed from a skin incision of approximately 1.5–2 cm. PC was opened and bluntly dissected from the deep fascia to create pockets of approximately 1 cm before inserting the cylinders between the PC and the fascia (Figure 2f). The pockets were then individually closed with sutures to immobilize the implants before suturing the skin. Additionally, a piece of autologous cartilage was harvested similarly to the cartilage biopsies, as described above, and transplanted together with the TE cylinders as a control. In summary, each animal received the following transplants: 1) autologous TE construct, 2) acellular construct, 3) two pieces of autologous auricular cartilage transplant (Figure 2b).

All rabbits were administered Buprenorphine 0.05 mg kg^{-1} every 12 h for postoperative analgesia. Wound healing and general conditions (e.g., weight, activity) of the animals were monitored daily. The experiment was terminated under general anesthesia (MMF s.c.) by injection of Pentobarbital 400 mg kg^{-1} through the ear vein. A fresh piece of auricular cartilage was harvested from the sacrificed animals as a reference tissue in addition to the transplants.

2.2. Chondrocyte Isolation

Auricular cartilage biopsies were diced with a sterile scalpel and/or surgical scissors, washed with sterile DPBS, and suspended in cell culture medium (DMEM/F12 + GlutaMAX, Gibco) supplemented with 10 % FBS, 0.05 mg mL^{-1} Gentamicin, and 0.1% Collagenase Type II (Gibco, ThermoFisher Scientific). The samples were then incubated overnight at 37 °C on a plate shaker and passed through a cell sieve (100 µm) to separate the cells from the digested tissue debris. The isolated cells were cultured in DMEM/F12 (GlutaMAX) supplemented with 10 % FBS, 0.05 mg mL^{-1} Gentamicin, 10 ng mL^{-1} TGF β3 (Proteintech), and 10 ng mL^{-1} FGF-2 (Peprotech) at 37 °C and 5% CO_2 until 90% confluency.

All surgical procedures, chondrocyte isolation, and their initial culture were performed at the Department of Otorhinolaryngology, Head and Neck Surgery, University Clinic Mannheim. The cultured cells in passage (P) 1 were transported to the Tissue Engineering and Biofabrication Laboratory, Institute for Biomechanics, ETH Zurich for further expansion and bioprinting.

2.3. Cell Culture

At the TE and Biofabrication Laboratory, P1 chondrocytes were further expanded until P3 in expansion medium composed of DMEM (31 966, Gibco) supplemented with 10% FBS (10270-106, Gibco), 10 µg mL^{-1} gentamycin (15710-049, Gibco), 10 ng mL^{-1} FGF-2 (100-18B, PeproTech), and 10 ng mL^{-1} TGF-β3 (AF-100-36E, PeproTech). During passaging, cells were trypsinized (0.25% Trypsin-EDTA (1x), Gibco) for 5 min, centrifuged at 500 rcf for 4 min, the cell pellet resuspended in expansion medium, and cells seeded at a density of 3000 cells cm^{-2}. At confluency, cells were trypsinized for 5 min, collected, centrifuged at 500 rcf for 4 min, and seeded again at 3000 cells cm^{-2}. At P3, cells were collected and combined with the bioink as described below. Cell expansion was carried out at 95% humidity, 5% CO_2 and 37 °C.

2.4. Bioprinting

From each biopsy, separate constructs were bioprinted for transplantation and for in vitro tests to assess the degree of construct maturation.

Bioink preparation: The HATG bioink was prepared as reported previously.[23] Briefly, 5.02% poly-n-acetyl glucosamine nanofibrils (Marine Polymer Technologies Inc., USA) were dispersed in TRIS buffered glucose (TBG, 50×10^{-3} M TRIS (Tris-(hydroxymethyl)-aminomethane), 200×10^{-3} M d-glucose, pH 7.6) by sonication (Branson 2510EMTH) and combined with 1.21% HA (HA15M-5, Lifecore Biomedical) in TBG 1:1. Following HA, HATG and alginate (UP LVG alginate, Pronova) were sequentially added to slowly raise the bioink's viscosity. The bioink stock was then combined with factor XIII (FXIII, Fibrogammin, CSL Behring), thrombin (TISSEEL, Baxter), and cells to reach a final concentration of 0.5% HATG, 0.25% Alg, 1.5% HA, 2.0% sNAG, 20 U mL^{-1} FXIII, 1 U mL^{-1} thrombin, and 30×10^6 rabbit auricular chondrocytes (rAUR) mL^{-1}. Before combining cells with the bioink, cells were washed twice with TBG to avoid any calcium ions within the bioink.

Bioprinting: Bioprinting was carried out on a Biofactory bioprinter (regenHU). Gcode was generated in Slic3r (v1.3.0) and postprocessed with a custom-written MATLAB script (MATLAB 2020b). Pneumatic extrusion at a pressure of ≈40–50 kPa together with a 410 µm tapered nozzle was used to print the constructs onto microscopy glass slides. Postprinting, slides were transferred into 50 mL Falcon tubes filled with 100×10^{-3} M $CaCl_2$ to initiate enzymatic cross-linking according to the calcium-triggered enzymatic cross-linking (CTEC) process described previously.[23] Constructs were cross-linked for 90 min and transferred into well plates for culture. Two types of cylindrical constructs were printed. The cylinders with a diameter of 6 mm and a height of 1 mm were printed for the in vitro analysis before implantation. The samples used for the in vivo implantation had a diameter of 10 mm and a height of 1 mm. Cultivation was performed in a chondrogenic medium composed of DMEM (31 966, Gibco) supplemented with 1% ITS (41400-045, Gibco), 50 µg mL^{-1} L-ascorbate-2-phosphate (A2521, TCI), 40 µg mL^{-1} L-proline (P5607, Merck), 10 µg mL^{-1} gentamycin (15710-049, Gibco), and 10 ng mL^{-1} TGF-β3 (AF-100-36E, PeproTech) at 95% humidity, 5% CO_2, and 37 °C. Construct maturation was evaluated after 3 and 9 weeks in vitro and after 14 weeks in vivo. The handling of the constructs was performed in sterile conditions under a laminar flow hood and the monitoring of cultured constructs was regularly performed to ensure the absence of bacterial or fungal contamination.

2.5. Viability

Viability was assessed on days 1 and 21. Gels were washed three times in media (DMEM 31 966, Gibco) and afterwards incubated

in 1×10^{-6} M CalceinAM (C3099, Thermo Fisher) and 1×10^{-6} M propidium iodide (81 845, Fluka) in media (DMEM 31 966, Gibco) for 1 h. Following staining, gels were washed three times and imaged on a Leica SP8 multiphoton microscope equipped with a 25× water immersion objective. CalceinAM excitation was carried out at 900 nm (Mai Tai XF, Spectra- Physics) while propidium iodide excitation was carried out at 1100 nm (InSight DeepSee, Spectra- Physics). CalceinAM emission was collected from 500 to 570 nm and propidium iodide emission from 695 to 740 nm. Simultaneously, the second harmonic generation (SHG) signal was collected from 442 to 458 nm. Gels were imaged from their surface 100 µm into the gel with 1 µm steps. Viability was calculated by dividing the number of viable cells (CalceinAM) by the number of total cells (viable and dead cells – propidium iodide). At each timepoint, three gels per donor were stained, and 10 donors were analyzed, including four donors from the in vivo experiment and six additional donors which were used to analyze tissue maturation in vitro (Figure 1b).

2.6. Compression Test

Unconfined compression tests were carried out on a TA.XTplus Texture Analyzer (Stable Micro Systems) equipped with a 500 g load cell. To ensure full contact between the compression plates and the sample a pre-load was applied and samples were allowed to relax for 5 min. Samples were compressed to 15% strain at 0.01 mm s^{-1}. Loading and unloading curves were recorded and the compressive modulus was calculated by fitting the first 3% strain of the stress–strain curve.

2.7. Indentation Test

Indentation tests were carried out on a UNHT^3 Bio Bioindenter (Anton Paar). Samples were fixed on Petri dishes using superglue and submerged in 0.9% NaCl. Samples were indented with a spherical ruby indenter with a radius of 500 µm. A 15 µN contact force to detect the sample surface was applied followed by an indentation of 60 µm in 5 s. Force relaxation was measured for 300 s and each sample was indented on three different locations. Hertz modulus was calculated using the software's built-in analysis tool (Indentation 8.0.15, Anton Paar).

2.8. Histology and Immunohistochemistry of In Vitro Samples

In vitro samples were processed and analyzed at the Tissue Engineering and Biofabrication Laboratory, Institute for Biomechanics, ETH Zurich.

Embedding: Constructs were fixed in 4% paraformaldehyde for 4 h, washed three times in PBS, and dehydrated in a graded ethanol series. Paraffin embedding was performed on an automated tissue processor (Milestone LogosJ) followed by paraffin embedding. A total of 5 µm sections were cut on a microtome and sections were deparaffinized and rehydrated before staining. Three constructs per timepoint (3 and 9 weeks) were stained and rabbit auricular cartilage served as a positive control.

Safranin O: Safranin O staining was performed following standard protocols. Briefly, sections were stained in Weigert's Iron Hematoxylin (HIT107 & HIT109, Merck) for 5 min, washed in deionized water, differentiated in 1% acid alcohol (1% hydrogen chloride in 70% ethanol) for 2 s, washed, stained in 0.02% Fast Green (F7252-5G, Merck) for 1 min, destained in 1% acetic acid and finally stained in 1% Safranin O (S8884-25G, Merck) for 30 min. Afterwards, sections were dehydrated to xylene and mounted.

Elastin: Elastin staining was performed according to the manufacturer's instructions (Elastin Stain Kit, HT25A-1KT, Merck).

Immunohistochemistry: Antigen retrieval was performed with hyaluronidase (2000 units mL^{-1}, hyaluronidase from bovine testes, H3506-1G, Merck) at 37 °C for 30 min. Sections were washed and blocked with 5% bovine serum albumin (A13191, PanReac) in PBS for 1 h. Afterwards, sections were incubated with the primary antibody (collagen I: ab6308, 1.3 µg mL^{-1}, Abcam, collagen II: II-II6B3, 3.75 µg mL^{-1}, DSHB Hybridoma Product, deposited by Linsenmayer, T.F.) diluted in 1% BSA at 4 °C overnight. Next, sections were washed in 0.3% H_2O_2 for 15 min and incubated with the secondary antibody (Goat anti-mouse IgG-HRP, ab6308, 2 µg mL^{-1}, Abcam) for 1 h. Chromogen was developed using the DAB substrate kit (ab64238, Abcam) according to the manufacturer's instructions. Sections were stained in Weigert's iron hematoxylin, destained in 1% acid alcohol for 2 s, and blued in 0.1% Na_2CO_3 for 1 min. Afterwards, sections were dehydrated to xylene and mounted.

Imaging: Brightfield imaging was performed on an automated slide scanner (Panoramic 250, 3D Histech).

2.9. Histology and Immunohistochemistry of In Vivo Samples

Explantation and analysis of the in vivo samples were performed at the Department of Otorhinolaryngology, Head and Neck Surgery, University Clinic Mannheim. The explanted cylinders with the surrounding tissues were fixed in 4% Formalin pH 7.4 for 48 h and embedded in paraffin. Paraffin sections (5–7 um) were deparaffinized and stained with hematoxylin and eosin (H&E) for biocompatibility analysis. Sulfated glycosaminoglycans (GAGs) were visualized by Alcian blue and Safranin O staining. Shortly, the sections were immersed into 1% Alcian blue solution in 3% acetic acid (pH 2.5) for 30 min at RT and transferred to 3% acetic acid for 1 min. The samples were then washed in distilled water for 2 min before counterstaining with 0.1% nuclear fast red (Sigma). For Safranin O staining, deparaffinized sections were first stained with hematoxylin followed by washing with water and incubated with Lightgreen (Goldner III) dye for 3 min. The samples were transferred into 1% acetic acid for 1 min and stained with 0.1% Safranin O aqueous solution for 6 min, finalized with a 10-s differentiation step in 1% acetic acid.

The elastic van Gieson (EVG) stain was performed to visualize elastin fibers. Deparaffinized samples were incubated in Resorcin–Fuchsin solution for 15 min and nuclei were counterstained with Weigert's iron hematoxylin solution for 15 min. The samples were washed and shortly suspended into hydrochloric acid alcohol (1%/70%) before staining with Van Gieson's Picrofuchsin solution for 1–5 min.

Immunohistochemistry was performed after antigen retrieval with citrate buffer pH 6.0 at 80 °C for 20 min. The sections were incubated with Proteinase K (Dako, Agilent, Germany) for

6 min and subsequently with endogenous peroxidase blocking solution (Dako, Agilent Technologies) for 30 min. Blocking was performed with 10% normal sheep serum for 30 min before incubating with primary antibodies against collagen type II (CIIC1, DSHB, IA, USA) 1:100, or collagen type I (NB600-450, Novus Biologicals, Germany) 1:100 at 4 °C overnight. The samples were then washed in PBS 0.1% Tween 20 before adding the secondary antibody (biotinylated anti-mouse IgG, Thermo Fisher Scientific) for 45 min. Subsequently, the sections were washed, streptavidin-biotinylated horseradish peroxidase complex (GE Healthcare) was applied and the samples were visualized with 3-amino-9-ethylcarbazole (AEC) peroxidase substrate solution (ScyTek Laboratories, Germany).

2.10. TUNEL Assay

To assess cell apoptosis in the explanted samples, terminal deoxynucleotidyl transferase-mediated dUTP nick-end labeling (TUNEL) of fragmented nuclear DNA was performed on deparafinized tissue sections using DeadEnd Colorimetric TUNEL System (Promega, Germany) according to manufacturer's instructions. Assay positive control was prepared by incubating auricular cartilage sample with DNase for 10 min at room temperature to induce DNA fragmentation.

2.11. Biocompatibility Analysis

The assessment of in vivo biocompatibility of all scaffolds and the autologous control was performed according to ISO 10993–6:2016 of the biological assessment of medical devices (Biological evaluation of medical devices – Part 6: Tests for local effects after implantation). Histological parameters, such as encapsulation, presence of polymorphonuclear leukocytes, lymphocytes, plasma cells, macrophages and giant cells, along with necrosis, neovascularization, fatty infiltration, and fibrosis were assessed to obtain a semiquantitative biocompatibility score. The score of each sample was then normalized to the autologous control, and the degree of irritation was classified as minimal (0–2.9 points), slight (3–8.9 points), moderate,[9–15] or strong (>15.1), as defined by the ISO standard. The statistical significance of differences between the irritation caused by cell-laden and acellular constructs was determined by a two-tailed *t*-test using GraphPad Prism Software (CA, USA).

3. Results

3.1. Animal Surgery

One animal died during narcosis while obtaining the biopsy. In the remaining three rabbits, surgeries and the postoperative period were without complications. No visible swelling, seromas, or inflammation were observed. The site of the biopsy, as well as the site of the implantation, healed well, and rabbits were active throughout the entire postoperative period.

3.2. Maturation of Bioprinted Constructs In Vitro

Control cylinders were printed to evaluate cell viability and construct maturation in vitro for up to 9 weeks, similar to our previous study.[23] Postprinting 75 ± 6% of cells was viable, which remained unchanged after 21 days (77 ± 7%, **Figure** 3a,b). Biomechanically, the stiffness of the constructs increased from 9 ± 1 to 167 ± 28 kPa in compression and from

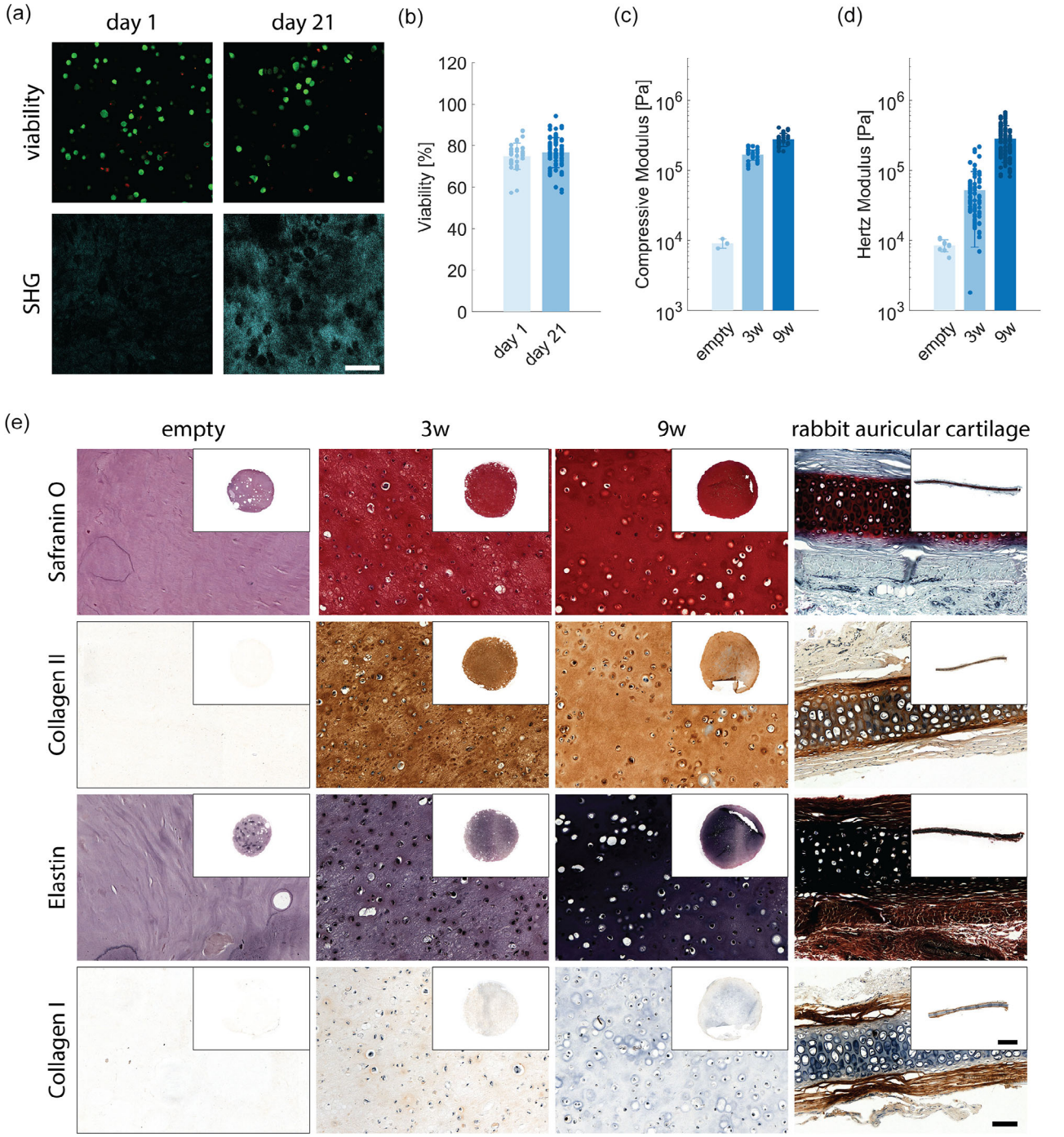

Figure 3. In vitro maturation of control cylinders. a) Cell viability (green: viable cells, red: dead cells) and second harmonic generation (SHG) at days 1 and 21 after printing. Scale bar: 100 µm. b) Cell viability was calculated from viability images by counting viable and dead cells. c) Compressive and d) Hertz modulus of control cylinders after 3 and 9 weeks of maturation compared to acellular (empty) constructs. e) Histological and immunohistological stainings for glycosaminoglycans (GAGs; Safranin O), elastin, collagen I, and collagen II after 3 and 9 weeks of maturation compared to acellular (empty) samples and rabbit auricular cartilage. Scale bar: close up: 100 µm, full view: 2 mm. $n = 3$ per donor, 10 donors.

8.6 ± 1.6 to 52 ± 44 kPa in indentation (Hertz modulus) after 3 weeks. After 9 weeks, the increase in compression and indentation values in the TE constructs amounted to 277 ± 60 and 282 ± 153 kPa, respectively (Figure 3c,d), falling short of the stiffness of native rabbit auricular cartilage, which measured 514 ± 180 kPa in compression and 2599 ± 830 kPa in indentation (Figure 5b,c).

Histologically, constructs showed the deposition of GAGs and collagen II after 3 weeks followed by the deposition of elastin

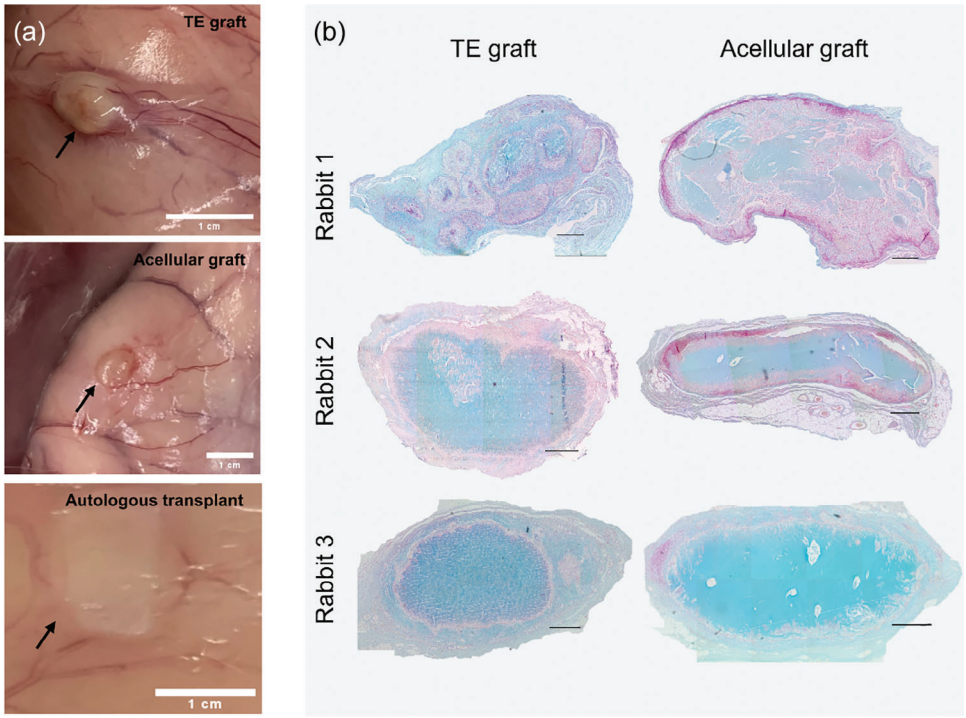

Figure 4. In vivo cylinder explants. a) Representative pictures of cylinders with (top) or without cells (middle) and autologous cartilage (bottom) 14 weeks after implantation between panniculus carnosus (PC) and the deep fascia. Arrows indicate the location of transplants. b) Alcian blue staining of tissue-engineered (TE) cylinders 14 weeks postimplantation. Scale bar 500 µm.

visible after 9 weeks (Figure 3e). No collagen I deposition was observed, indicating the maturation toward auricular cartilage rather than fibrocartilage. However, the elastin network in constructs did not show the same complex architecture and long elastin fibers observed in native rabbit auricular cartilage.

3.3. General Observations and Histology of the Implants

Pronounced vascularization was often visible around the implanted scaffolds, but much less so in the autologous control (**Figure** 4a). Histological overview revealed some degree of degradation in every scaffold; however, degradation was most severe in one animal with partial disintegration of both cell-laden and cell-free scaffolds inside the fibrous capsule (rabbit 1, Figure 4b).

All scaffolds were distinguishable with Alcian blue staining (Figure 4b). However, there was no clear difference in the staining intensity between cell-laden and cell-free implants. Safranin O, in contrast, was negative in both cell-laden and cell-free scaffolds after transplantation, whereas clear metachromasia was visible in the autologous control and native auricular cartilage (**Figure** 5a). Similarly, collagen type II was absent in all TE scaffolds, in contrast to the autologous control (Figure 5a). Collagen type I was visible in the fibrous capsule surrounding the TE cylinders, as well as in the autologous control (Figure 5a). However, the morphology of the collagen type I-positive tissue in the autologous control was different from the fibrous capsule, resembling fibrous perichondrium, possibly partly retained on the autologous cartilage during transplantation. No elastin fibers were observable in the TE samples, however, elastin staining was also reduced in the autologous transplant compared to freshly harvested auricular cartilage, which was used as a reference (Figure 5a). Mechanically, autologous transplants were significantly softer than native auricular cartilage in indentation and showed a trend toward becoming softer in compression (Figure 5b,c). Additionally, the analysis of the loading-unloading stress–strain curves of compression tests showed the dissipation of more strain energy by autologous transplants as compared to the native tissue (Figure 5d,e), indicating the loss of elasticity in autologous transplants. TE samples lacked mechanical integrity for testing. Other parameters, such as staining against collagens type I and II, or the presence of sulfated GAGs were comparable in autologous transplants and native auricular cartilage, with only minor differences attributable to variations in histological procedures.

3.4. Biocompatibility Analysis

Peripheral degradation and immune cell infiltration were observed in all samples (Figure 4b and **Figure** 6a). In rabbit 1, pieces of the disintegrated scaffold were densely surrounded by immune cells (Figure 4b). In rabbit 2, only one region of degradation away from the periphery was observed, whereas only peripheral degradation could be seen in the third animal. Notably, no neovascularization of any implant was observed in rabbit 1, while some neovascularization was present in all TE samples in the other two animals (**Table** 1). Neovascularization was absent in autologous control samples in all rabbits. All types of immune cells analyzed for evaluation of biocompatibility were present in the immune infiltrates. No immune infiltra-

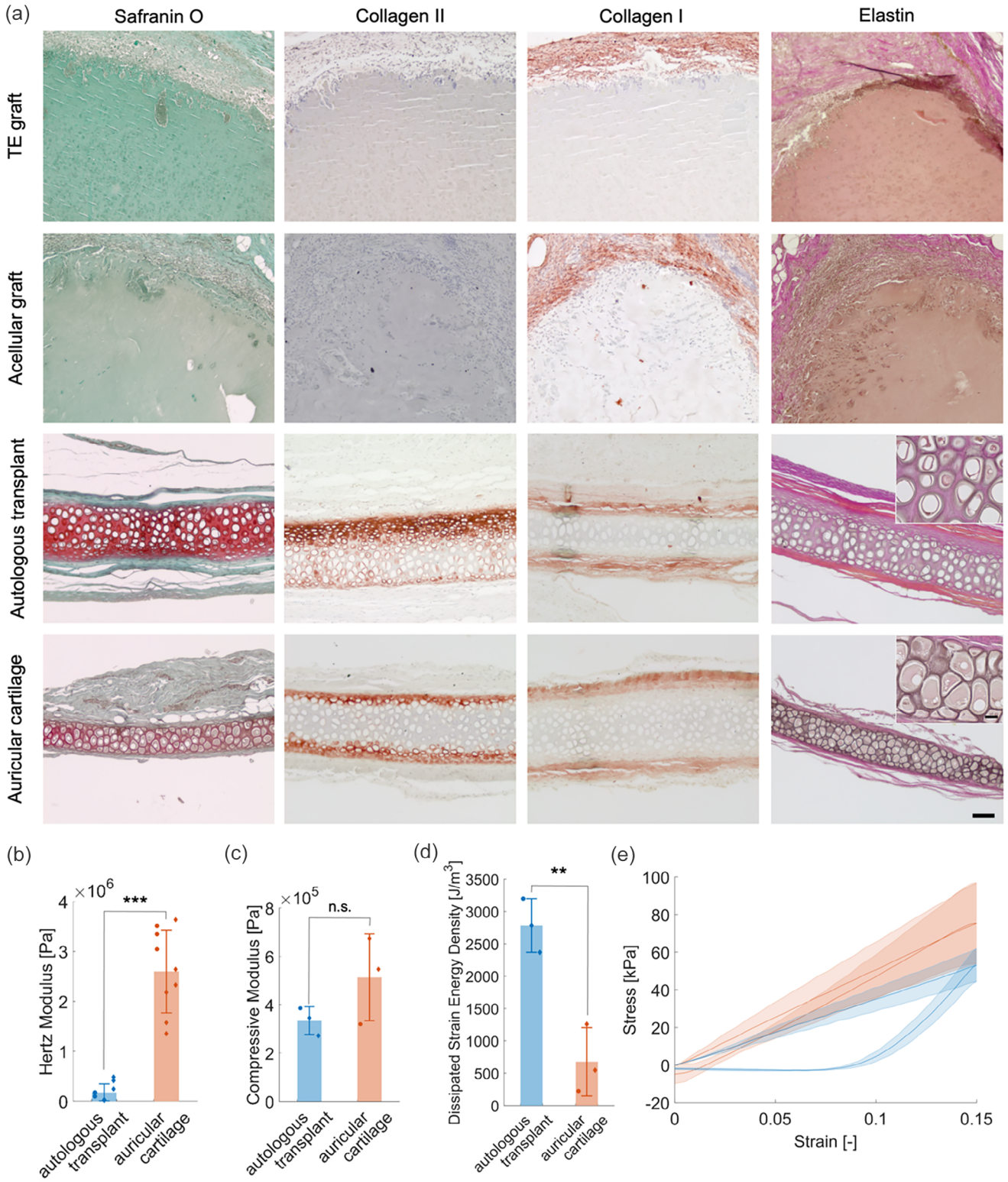

Figure 5. Histology and mechanical characterization. a) Micrographs depicting histological staining for sulfated glycosaminoglycan (GAGs; Safranin O/Fast green), collagen type II, collagen type I, and elastin (Van Gieson) 14 weeks after implantation of tissue-engineered (TE) constructs as compared to the autologous transplant and native auricular cartilage. Staining of elastic fibers depicts no staining in implants and a scarce presence of elastic fibers in the autologous transplant as compared to the freshly harvested auricular cartilage. Scale bar 100 and 20 µm (Van Gieson's elastic stain insets). b) Hertz modulus and c) compressive modulus. d) Dissipated strain energy density calculated from stress–strain curves (e). $^{*}p < 0.05$, $^{**}p < 0.01$, $^{***}p < 0.001$,unpaired *t* test.

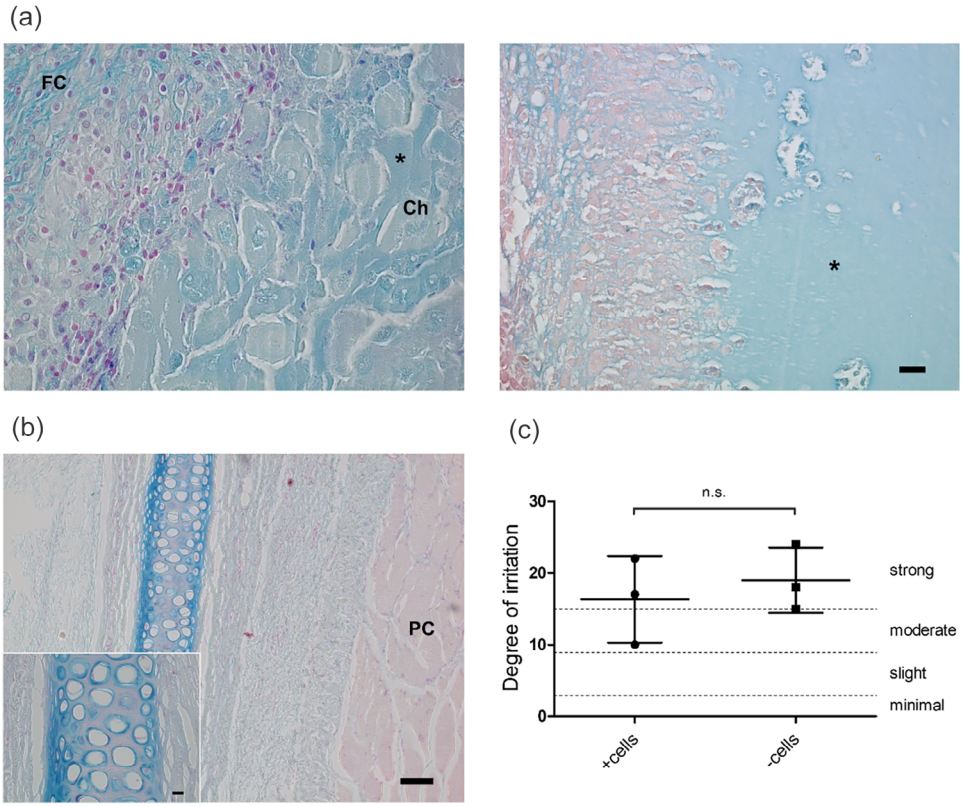

Figure 6. Implant biocompatibility. a) Representative micrographs of cell-laden (left) and cell-free (right) grafts (asterisk) after 14 weeks in vivo. Degradation and immune cell infiltration originating from the fibrous capsule (FC) are visible at the scaffold periphery. Chondrocytes (Ch) are distinguishable in the cell-laden scaffold. Scale bar 20 µm. b) Autologous cartilage placed between the panniculus carnosus (PC) and deep fascia shows no signs of immune infiltration or degradation. Scale bar 100 µm, inset 20 µm. c) A semiquantitative score indicates the degree of irritation of the host tissues by the implants relative to the autologous controls. Data from Table 1 is depicted as mean ±SD from three experimental animals, normalized by subtraction of the respective autologous control scores.

tion was observed in autologous controls (Figure 6b and Table 1). Macrophages, including foreign body giant cells, were around the TE scaffolds in the highest numbers in rabbit 1, where degradation was most prominent. A higher prevalence of lymphocytes was observed in the acellular transplants, possibly indicative of an increased involvement of the adaptive immune response. Overall, the host immune response ranged from moderate to strong irritation, being slightly less in TE scaffolds with cells (Figure 6c).

TUNEL assay revealed DNA fragmentation within the TE grafts, suggesting that the embedded cells underwent apoptosis and were no longer viable at the time of explantation (Figure S1a). In contrast, only scarce peripheral staining was visible in the autologous transplant (Figure S1b) and native auricular cartilage

Table 1. Evaluation of biocompatibility.

PC	Implant	PMNC	LC	PC	Macro-phages	GC	Necrosis	Subtotal (x2)	NV	Fibrosis	FI	Subtotal	Total
Rb 1	+cells	2	2	2	2	0	0	16	0	2	0	2	17
	−cells	1	3	2	3	3	0	24	0	1	0	1	24
	Autolog.	0	0	0	0	0	0	0	0	1	0	1	–
Rb 2	+cells	2	2	2	1	1	3	22	1	0	0	1	22
	−cells	1	3	2	1	0	0	14	1	1	0	2	15
	Autolog.	0	0	0	0	0	0	0	0	1	0	1	–
Rb 3	+cells	1	1	1	1	0	1	10	1	1	0	2	10
	−cells	1	3	1	1	0	2	16	1	2	1	4	18
	Autolog.	0	0	0	0	0	0	0	0	2	0	2	–

Semiquantitative scores based on histological parameters. Autologous control scores from each animal were subtracted to show the relative biocompatibility of the constructs. PMNC, polymorphonuclear cells; LC, Lymphocytes; PC, plasma cells; GC, giant cells; NV, neovascularization; FI, fatty infiltration.

(Figure S1c), whereas DNase treatment (positive control) resulted in DNA fragmentation and increased staining (Figure S1d).

4. Discussion

Engineering a TE-auricle that can withstand transplantation to immunologically active environments is one of the main challenges in the field. Currently, autologous animal models are the only way to predict the behavior of a TE construct after transplantation in a clinical setting. In our experiment, we used an autologous rabbit model to evaluate the stability of TE cartilage consisting of an HATG-based bioink and autologous auricular chondrocytes. Overall, a moderate to strong immune response with typical characteristics of foreign body response, such as fibrous encapsulation, immune cell infiltration, and partial scaffold degradation with the loss of key ECM components were observed in both the acellular graft and the TE-construct. For most scaffolds, we observed only peripheral degradation adjacent to the fibrous capsule, where the immune cell infiltration had occurred. In one animal, degradation and immune cell infiltration were more pronounced compared to the other recipients. This could be due to the individual characteristics of the immune system or a technical issue (e.g., insufficient fixation of the implants beneath the PC, wider PC pocket, etc.) while establishing the implantation technique intraoperatively in the first animal. The distinctive absence of neovascularization of TE implants in this recipient (Table 1) could also be pointing to a relatively loose contact of the implants with the vascularized PC.

Animal models come with limitations with regard to species-related differences in terms of the TE cartilage quality, as well as the anatomy and physiological response to transplantation. The choice of animal in our study was determined by similarities between human and rabbit auricular cartilage,[28] as well as practical reasons, such as availability, the ease of housing, good donor source of autologous auricular chondrocytes, and less ethical concern than that associated with the use of larger animals. Notably, the use of the rabbit model in articular cartilage TE research is controversial due to the increased spontaneous healing of osteochondral defects compared to humans.[29] However, the extensive analysis of the regeneration mechanism of osteochondral defects in rabbits has concluded that the repair of articular defects in rabbits is entirely mediated by the proliferation and differentiation of mesenchymal cells from the adjacent bone marrow, with no contribution from the residual cartilage.[30] Similarly, in auricular cartilage, in rabbits, as well as in humans, the formation of de novo cartilage originates from perichondrium with no intrinsic regenerative capacity of the cartilage tissue itself.[31] These similarities to the human auricular cartilage combined with practical benefits have rendered the rabbit model historically popular for investigating auricular cartilage regeneration.[31] Furthermore, rabbit auricular cartilage has been described to resemble human tissue in terms of GAG and collagen content, as opposed to some larger animal species, such as pig and cow.[28] Naturally, there are also significant differences between rabbit and human auricular cartilage, such as those in size, cell density, and morphology of chondrocytes,[28] suggestive of functional interspecies distinctions between the cells, which need to be taken into account when interpreting the results of the translational model.

Alternative cell sources, such as chondroprogenitors, or a combination of chondrocytes with mesenchymal stem cells have been proposed for auricular cartilage TE, with favorable results in terms of mechanical and biochemical composition of the obtained cartilage tissue.[26,32,33] However, in our study, autologous auricular chondrocytes were chosen as they represent the residing cells in the auricle, have the potential to regenerate elastic cartilage, and can be obtained from a small (e.g., a 6 mm) biopsy. In the case of unilateral microtia (90% of the cases) auricular chondrocytes can be obtained from the healthy ear, whereas for bilateral microtia, microtic chondrocytes or costal chondrocytes represent valuable cell sources but require further investigation.

Rabbits have been previously used as an autologous immunocompetent model for TE cartilage made of various materials.[9,13] A similar model has been used by Shieh et al. for autologous cartilage engineered with three types of synthetic materials – PGA, PCL, and poly-4-hydroxybutyrate (P-4HB). Comparably to our experiment, autologous TE constructs were precultured for 8 weeks and transplanted beneath the PC on the back of the rabbits for 3 months. Regardless of the polymer type, severe foreign body response, with immune cell infiltration and implant deformation was observed in all constructs in this study. Similarly, two-stage implantation of autologous TE cartilage made of PGA and poly-L-lactic acid (PLLA) into the dorsum of the rabbits in another study also resulted in the eventual loss of shape, mass, cellular integrity, and positive GAG staining.[13] The inflammatory response to PGA in combination or without other synthetic materials, such as polylactic acid (PLA) has also been reported in other autologous models besides rabbits, including sheep[34] or pigs.[35] However, a favorable outcome has been reported with the same material, when a PGA/PLA construct was transplanted at the anterior neck of the rabbits after a 4-week preculture with autologous auricular chondrocytes.[12] Furthermore, PGA/PLA-based autologous TE-cartilage has been used for the reconstruction of the human auricle in pediatric microtia patients, with no significant deformation after a 12-month follow-up.[6] These conflicting reports suggest that material might not be the sole reason for implant rejection observed in the autologous rabbit model. Shieh et al. proposed that soft tissue contraction and characteristics of rabbit skin structure could have contributed to the severe foreign body response, which occurred regardless of the biomaterial type in their study.

The site of transplantation is known to be one of the key determinants of immune rejection. While subcutaneous transplantation is most commonly employed, it is also known to trigger the most severe immune response.[10] Implanting a TE construct into its native site may result in a radically different outcome as opposed to subcutaneous transplantation. This is illustrated by articular cartilage reconstruction in the autologous porcine model, where engineered chondrocyte-PGA cartilage formed histologically compatible tissue when transplanted to the defect created in the articular cartilage,[36] but developed into fibrocartilage when transplanted subcutaneously.[15] In our experiment, we used transplanted autologous auricular cartilage as a control to exclude the influence of the implantation site on the cartilage constructs. Overall, the autologous auricular cartilage structure was mostly intact. However, the loss of elastin fibers as compared to the freshly harvested auricular cartilage (Figure 5a) could account for the differences between the native and transplantation

environments. This observation was supported by the decline of mechanical properties (Figure 5b,c) as well as the drastic increase in dissipated strain energy (Figure 5d,e) underlining the loss of elastic behavior of the autologous implants. Overall, the implantation of TE grafts in their native site could have a positive impact on the local tissue response. However, it is often technically challenging in animals, due to the accessibility of the transplantation site to self-induced damage (e.g., by scratching or biting), as well as the possible insufficiency of local vascularization required to promote graft maintenance.

In our experiment, the constructs were transplanted beneath the PC, rather than directly subcutaneously. PC is a vascularized striated muscle located between the skin and deep fascia and is highly conserved across mammals, with some primates, including humans, being an exception.[37] PC has been a favored transplantation site in rodents due to its extensive vascularization and graft maintenance, but also relative immune privilege as compared to the skin tissue.[38] However, rabbits differ from rodents in this respect. In contrast to rats or guinea pigs, rejection of skin allografts occurs as promptly when transplants are placed on rabbit PC as when they are in contact with the host skin tissue. In rodents, the immune privilege of PC is thought to be caused by disruption of the lymphatic network during the preparation of the PC bed, whereas in rabbits, dissection of skin and PC leaves the lymphatic and vascular network intact due to a natural cleavage site between dermis and PC.[38] Finally, mobility and contraction of PC may be a contributing factor to the poor performance of TE grafts in our and others' transplantation model; contraction for maintenance of body temperature (shivering thermogenesis) or skin twitching as a defense mechanism against irritants are among the key functions of PC.[37] The aspect of mobility and contraction would be naturally absent in a clinical scenario of graft transplantation in humans, where a vascularized fascial flap would be positioned between the skin and transplant.[39] as opposed to a muscular structure like PC.The HA used in our scaffolds could have also contributed to the observed immune reaction. HA plays a critical role in modulating the inflammatory response in which high molecular weight HA is known to be anti-inflammatory, and low molecular weight HA is thought to elicit various proinflammatory processes.[40,41] While we used high molecular weight-HA as starting material, degradation could have reduced its molecular weight leading to low molecular weight fragments that elicited an inflammatory response in the surrounding tissue. Whether high molecular weight-HA was still present at the implantation, particularly in matured TE grafts, or whether it was degraded in vivo and impacted the immune response, remains an open question.

In our samples, we observed a complete loss of cartilage histological markers, including GAGs, collagen type II, and elastin, as well as apoptosis of the embedded autologous cells within the TE grafts. A possible explanation of these phenomena could be the diffusion of the inflammatory factors secreted by the immune cells resulting in the degradation of the deposited ECM and the loss of chondrocyte viability. Furthermore, as mentioned above, the reduction of the elastic fibers combined with the loss of elasticity also occurred in autologous cartilage transplants regardless of the absence of immune cell infiltration. This suggests the implication of additional factors at the transplantation site that affected transplant ECM. However, unlike TE transplants, autologous cartilage transplants were covered by the perichondral layer (Figure 5a), apparently partly retained after dissection during the surgical procedure. The perichondral layer could have offered partial protection to the autologous cartilage tissue from the diffusion of any factors affecting the ECM, in addition to preventing the immune infiltration, as previously described.[13] However, at this point, it is overall unclear whether the diffusion of proteolytic factors could be sufficient to cause such dramatic degradation of the ECM during the 14-week implantation period, or whether and to what degree the embedded cells contributed to the disappearance of the cartilage markers in the TE grafts. A more dynamic study with multiple early explantation time points is necessary to address these questions.

Due to the problematic outcomes of autologous graft transplantation in rabbits, some authors have advocated using sheep as an autologous animal model of auricular cartilage reconstruction. In studies using an ovine model, TE grafts composed of fibrous collagen scaffolds and autologous auricular chondrocytes were implanted subcutaneously for 12 weeks.[10,17] While small cylindrical grafts were able to maintain their shape,[10] larger auricular grafts required a titanium wire framework and showed deformation around the titanium wire.[17] Another recent publication reported the transplantation of autologous auricular TE cartilage for 12 weeks in a rabbit model.[42] Since the primary focus of the study was to assess noninvasive monitoring of graft maintenance using magnetic resonance imaging, limited information was provided regarding the immune response and biocompatibility. Nevertheless, the authors reported overall maintenance of the transplant shape. Interestingly, partial resorption of autologous control transplants was observed in this study, which aligns with the loss of elasticity seen in our experiments with autologous transplants.

5. Conclusion

Our work emphasizes the importance of autologous animal models as a principal preclinical test for TE constructs and illustrates the urgent need for an in-depth understanding of the host response to autologous TE products. In summary, it appears important to achieve a sufficient maturation of TE constructs before implantation to ensure in vivo shape stability as observed in our autologous implants. However, softening of the autologous implants also implies a more complex immune response toward these implants. Therefore, managing the inflammatory response to preserve these implants could be instrumental. Studies have shown that size, shape, and stiffness are important in managing the inflammatory response.[43,44] Additionally, the adsorption of plasma proteins following implantation is crucial for the inflammatory response which can lead to fibrous encapsulation.[45] Particularly, the partially retained perichondrial layer might have provided additional protection to autologous transplants. Specifically for our material, degraded low-molecular weight HA could also be a contributing factor to the inflammatory response. Considering the Good Manufacturing Practice (GMP) standards, such as preparation of biomaterials in dust-free clean rooms and sterile handling of TE constructs could significantly aid in the mitigation of immune response but is not always feasible in academic labs. Furthermore, to preserve TE grafts, immunomodulatory approaches to achieve biomate-

rial/graft tissue integration such as the inclusion of triazole surface modifications[46] or coating with zwitterionic materials.[47,48] could be implemented. Moreover, coating the constructs with a soft hydrogel layer or TE perichondrium could overcome the mismatch in mechanical properties. Lastly, the species-specific foreign body response and wound healing response could play an important aspect in testing TE grafts.[49,50] Other species, such as sheep might be better suited as autologous models for auricular cartilage reconstruction. In conclusion, further investigation will be needed to better understand the host immune response to TE cartilaginous grafts.

Supporting Information

Supporting Information is available from the Wiley Online Library or from the author.

Acknowledgements

D.G. and P.F. contributed equally to this work. The authors gratefully acknowledge the excellent support of the Core Facility of Preclinical Models, Medical Faculty Mannheim, and Petra Prohaska, MTLA for preparing the histological sections. The authors acknowledge ScopeM (ETH Zürich) for their support and assistance in this work. The project was funded by the Swiss National Science Foundation (CRSII5_173 868).

Open access funding enabled and organized by Projekt DEAL.

Conflict of Interest

The authors declare no conflict of interest.

Data Availability Statement

Gvaramia D, Fisch P, Flégeau K, Huber L, Kern J, Jakob Y, Hirsch D, Rotter N, 2023, https://doi.org/10.11588/data/0BQTPT, heiDATA.

Keywords

auricular reconstruction, autologous animal model, bioprinting, cartilage tissue engineering, enzymatically cross-linked hydrogels

Received: January 3, 2024
Revised: February 16, 2024
Published online:

[1] N. Rotter, A. Haisch, *Eur. Arch. Oto-Rhino-Laryngol.* **2005**, *262*, 539.
[2] Z. M. Jessop, M. Javed, I. A. Otto, E. J. Combellack, S. Morgan, C. C. Breugem, C. W. Archer, I. M. Khan, W. C. Lineaweaver, M. Kon, J. Malda, I. S. Whitaker, *Stem Cell Res. Ther.* **2016**, *7*, 19.
[3] S. Humphries, A. Joshi, W. R. Webb, R. Kanegaonkar, *Eur. Arch. Oto-Rhino-Laryngol.* **2022**, *279*, 541.
[4] D. A. Bichara, N.-A. O'Sullivan, I. Pomerantseva, X. Zhao, C. A. Sundback, J. P. Vacanti, M. A. Randolph, *Tissue Eng., Part B* **2012**, *18*, 51.
[5] I. A. Otto, F. P. W. Melchels, X. Zhao, M. A. Randolph, M. Kon, C. C. Breugem, J. Malda, *Biofabrication* **2015**, *7*, 032001.
[6] G. Zhou, H. Jiang, Z. Yin, Y. u. Liu, Q. Zhang, C. Zhang, B. o. Pan, J. Zhou, X. u. Zhou, H. Sun, D. Li, A. He, Z. Zhang, W. Zhang, W. Liu, Y. Cao, *EBioMedicine* **2018**, *28*, 287.
[7] W. Wei, Y. Ma, X. Yao, W. Zhou, X. Wang, C. Li, et al., *Bioact Mater* **2021**, *6*, 998.
[8] X. Dong, I. D. Premaratne, J. L. Bernstein, A. Samadi, A. J. Lin, Y. Toyoda, J. Kim, L. J. Bonassar, J. A. Spector, *Cartilage* **2021**, *13*, 1780S.
[9] S. J. Shieh, S. Terada, J. P. Vacanti, *Biomaterials* **2004**, *25*, 1545.
[10] D. A. Bichara, I. Pomerantseva, X. Zhao, L. Zhou, K. M. Kulig, A. Tseng, A. M. Kimura, M. A. Johnson, J. P. Vacanti, M. A. Randolph, C. A. Sundback, *Tissue Eng., Part A* **2014**, *20*, 303.
[11] W. Liu, Y. Cao, *Biomaterials* **2007**, *28*, 5078.
[12] X. Luo, G. Zhou, W. Liu, W. J. Zhang, L. Cen, L. Cui, Y. Cao, *Biomed. Mater.* **2009**, *4*, 025006.
[13] J. J. Christophel, J. S. Chang, S. S. Park, *Arch. Facial Plast. Surg.* **2006**, *8*, 117.
[14] A. Sterodimas, J. de Faria, *Aesthetic Surg. J.* **2013**, *33*, 283.
[15] Y. Cao, A. Rodriguez, M. Vacanti, C. Ibarra, C. Arevalo, C. A. Vacanti, *J. Biomater. Sci., Polym. Ed.* **1998**, *9*, 475.
[16] W. Xia, W. Liu, L. Cui, Y. Liu, W. Zhong, D. Liu, J. Wu, K. Chua, Y. Cao, *J. Biomed. Mater. Res., Part B* **2004**, *71B*, 373.
[17] I. Pomerantseva, D. A. Bichara, A. Tseng, M. J. Cronce, T. M. Cervantes, A. M. Kimura, C. M. Neville, N. Roscioli, J. P. Vacanti, M. A. Randolph, C. A. Sundback, *Tissue Eng., Part A* **2016**, *22*, 197.
[18] S. C. N. Chang, G. Tobias, A. K. Roy, C. A. Vacanti, L. J. Bonassar, *Plast. Reconstr. Surg.* **2003**, *112*, 793.
[19] A. B. Saim, Y. Cao, Y. Weng, C.-N. Chang, M. A. Vacanti, C. A. Vacanti, R. D. Eavey, *Laryngoscope* **2000**, *110*, 1694.
[20] B. N. Brown, B. D. Ratner, S. B. Goodman, S. Amar, S. F. Badylak, *Biomaterials* **2012**, *33*, 3792.
[21] N. Broguiere, E. Cavalli, G. M. Salzmann, L. A. Applegate, M. Zenobi-Wong, *ACS Biomater. Sci. Eng.* **2016**, *2*, 2176.
[22] E. Cavalli, P. Fisch, F. A. Formica, R. Gareus, T. Linder, L. A. Applegate, M. Zenobi-Wong, *J. Immunol. Regener. Med.* **2018**, *2*, 36.
[23] P. Fisch, N. Broguiere, S. Finkielsztein, T. Linder, M. Zenobi-Wong, *Adv. Funct. Mater.* **2021**, *31*, 2008261.
[24] D. Zielinska, P. Fisch, U. Moehrlen, S. Finkielsztein, T. Linder, M. Zenobi-Wong, T. Biedermann, A. S. Klar, *Sci. Adv.* **2023**, *9*, eadh1890.
[25] L. H. pyo, G. U. L., D. J. Mooney, M. E. Levenston, O. Chaudhuri, *Nat. Mater.* **2017**, *16*, 1243.
[26] B. P. Cohen, J. L. Bernstein, K. A. Morrison, J. A. Spector, L. J. Bonassar, *PLoS One* **2018**, *13*, e0202356.
[27] B. P. Cohen, R. C. Hooper, J. L. Puetzer, R. Nordberg, O. Asanbe, K. A. Hernandez, J. A. Spector, L. J. Bonassar, *Tissue Eng., Part A* **2016**, *22*, 461.
[28] L. L. Y. Chiu, R. Giardini-Rosa, J. F. Weber, S. L. Cushing, S. D. Waldman, *Ann. Otol., Rhinol., Laryngol.* **2017**, *126*, 819.
[29] C. R. Chu, M. Szczodry, S. Bruno, *Tissue Eng., Part B* **2010**, *16*, 105.
[30] F. Shapiro, S. Koide, M. J. Glimcher, *J. Bone Jt. Surg., Am. Vol.* **1993**, *75*, 532.
[31] D. Gvaramia, J. Kern, Y. Jakob, M. Zenobi-Wong, N. Rotter, *Tissue Eng., Part B* **2022**, *28*, 531.
[32] I. A. Otto, R. Levato, W. R. Webb, I. M. Khan, C. C. Breugem, J. Malda, *Eur. Cells Mater.* **2018**, *35*, 132.
[33] I. A. Otto, P. E. Capendale, J. P. Garcia, M. de Ruijter, R. F. M. van Doremalen, M. Castilho, T. Lawson, M. W. Grinstaff, C. C. Breugem, M. Kon, R. Levato, J. Malda, *Mater. Today Bio* **2021**, *9*, 100094.
[34] K. Kojima, L. J. Bonassar, A. K. Roy, C. A. Vacanti, J. Cortiella, *J. Thorac. Cardiovasc. Surg.* **2002**, *123*, 1177.
[35] N. Rotter, F. Ung, A. K. Roy, M. Vacanti, R. D. Eavey, C. A. Vacanti, L. J. Bonassar, *Tissue Eng.* **2005**, *11*, 192.
[36] Y. Liu, F. Chen, W. Liu, L. Cui, Q. Shang, W. Xia, J. Wang, Y. Cui, G. Yang, D. Liu, J. Wu, R. Xu, S. D. Buonocore, Y. Cao, *Tissue Eng.* **2002**, *8*, 709.

[37] N. Naldaiz-Gastesi, O. A. Bahri, A. López de Munain, K. J. A. McCullagh, A. Izeta, *J. Anat.* **2018**, *233*, 275.
[38] C. F. Barker, R. E. Billingham, *J. Exp. Med.* **1973**, *138*, 289.
[39] Y. Jaquet, K. M. Higgins, D. J. Enepekides, *Curr. Opin. Otolaryngol. Head Neck Surg.* **2011**, *19*, 235.
[40] M. Litwiniuk, A. Krejner, M. S. Speyrer, A. R. Gauto, T. Grzela, *Wounds* **2016**, *28*, 78.
[41] S. S. M. Lee-Sayer, Y. Dong, A. A. Arif, M. Olsson, K. L. Brown, P. Johnson, *Front. Immunol.* **2015**, *6*, 150.
[42] G. Yang, X. Li, W. Zhang, N. Wu, H. Chen, X. Liu, H. Jiang, *BMC Med. Imaging* **2023**, *23*, 36.
[43] A. Khademhosseini, R. Langer, *Nat. Protoc.* **2016**, *11*, 1775.
[44] O. Veiseh, J. C. Doloff, M. Ma, A. J. Vegas, H. H. Tam, A. R. Bader, J. Li, E. Langan, J. Wyckoff, W. S. Loo, S. Jhunjhunwala, A. Chiu, S. Siebert, K. Tang, J. Hollister-Lock, S. Aresta-Dasilva, M. Bochenek, J. Mendoza-Elias, Y. Wang, M. Qi, D. M. Lavin, M. Chen, N. Dholakia, R. Thakrar, I. Lacík, G. C. Weir, J. Oberholzer, D. L. Greiner, R. Langer, D. G. Anderson, *Nat. Mater.* **2015**, *14*, 643.
[45] C. Li, C. Guo, V. Fitzpatrick, A. Ibrahim, M. J. Zwierstra, P. Hanna, A. Lechtig, A. Nazarian, S. J. Lin, D. L. Kaplan, *Nat. Rev. Mater.* **2020**, *5*, 61.
[46] A. J. Vegas, O. Veiseh, J. C. Doloff, M. Ma, H. H. Tam, K. Bratlie, J. Li, A. R. Bader, E. Langan, K. Olejnik, P. Fenton, J. W. Kang, J. Hollister-Locke, M. A. Bochenek, A. Chiu, S. Siebert, K. Tang, S. Jhunjhunwala, S. Aresta-Dasilva, N. Dholakia, R. Thakrar, T. Vietti, M. Chen, J. Cohen, K. Siniakowicz, M. Qi, J. McGarrigle, A. C. Graham, S. Lyle, D. M. Harlan, et al., *Nat. Biotechnol.* **2016**, *34*, 345.
[47] L. Zhang, Z. Cao, T. Bai, L. Carr, J.-R. Ella-Menye, C. Irvin, B. D. Ratner, S. Jiang, *Nat. Biotechnol.* **2013**, *31*, 553.
[48] D. Dong, C. Tsao, H.-C. Hung, F. Yao, C. Tang, L. Niu, J. Ma, J. MacArthur, A. Sinclair, K. Wu, P. Jain, M. R. Hansen, D. Ly, S. G.-H. Tang, T. M. y. Luu, P. Jain, S. Jiang, *Sci. Adv.* **2021**, *7*, eabc5442.
[49] R. Whitaker, B. Hernaez-Estrada, R. M. Hernandez, E. Santos-Vizcaino, K. L. Spiller, *Chem. Rev.* **2021**, *121*, 11305.
[50] E. Mariani, G. Lisignoli, R. M. Borzì, L. Pulsatelli, *Int. J. Mol. Sci.* **2019**, *20*, 636.